First-principles study of diffusion of oxygen vacancies and interstitials in ZnO

2009 J. Phys.: Condens. Matter 21 195403

(http://iopscience.iop.org/0953-8984/21/19/195403)

J. Phys.: Condens. Matter **21** (2009) 195403 (6pp) doi:10.1088/0953-8984/21/19/195403

First-principles study of diffusion of oxygen vacancies and interstitials in ZnO

Gui-Yang Huang[1], **Chong-Yu Wang**[1,2] **and Jian-Tao Wang**[3]

[1] Department of Physics, Tsinghua University, Beijing 100084, People's Republic of China
[2] The International Centre for Materials Physics, Chinese Academy of Sciences, Shenyang 110016, People's Republic of China
[3] Institute of Physics, Chinese Academy of Sciences, Beijing 100080, People's Republic of China

Received 19 February 2009, in final form 18 March 2009
Published 16 April 2009
Online at stacks.iop.org/JPhysCM/21/195403

Abstract
A comprehensive investigation of oxygen vacancy and interstitial diffusion in ZnO has been performed using *ab initio* total energy calculations with both the local density approximation (LDA) and the generalized gradient approximation (GGA). Based on our calculation results, oxygen octahedral interstitials are fast diffusers, contributing to annealing processes, as well as being responsible for the self-diffusion of oxygen for n-type ZnO, and oxygen vacancies are responsible for the self-diffusion of oxygen for p-type ZnO.

(Some figures in this article are in colour only in the electronic version)

1. Introduction

Zinc oxide (ZnO), with wide bandgap (3.44 eV) and large exciton binding energy (60 meV), has attracted much interest for potential applications in optical and optoelectronic devices [1]. The diffusion behaviors of intrinsic point defects in ZnO are fundamentally and technologically important. The annealing behaviors of materials are determined by the diffusion of intrinsic point defects. The remarkable radiation hardness of zinc oxide is likely to be attributable to the annealing of defects by rapid defect migration [2]. Knowledge of the diffusion of point defects is important for the understanding of their incorporation during growth and processing, and it is essential for modeling self-diffusion and impurity diffusion. Generally, dopant atoms move only while they are in one of their defect states as follows: dopant interstitial A_i, dopant–vacancy pair AV or dopant–interstitial pair AI. The diffusion of dopant is mediated by the intrinsic point defect, so the diffusion behavior of vacancy and interstitial is essential for understanding the diffusion of dopant atoms. Several experiment studies [3–8] and theory studies [9, 10] have been conducted to study the self-diffusion of oxygen in ZnO. However, the experiment results exhibit a considerable spread, and no consensus has been reached. Since the activation energy for self-diffusion is the sum of the formation energy of the defect that mediates the self-diffusion and its migration energy barrier [11], it is not straightforward to interpret these results, in which the formation energy of the defect strongly depends on the experimental conditions, such as the position of the Fermi level and the zinc or oxygen chemical potentials, which can cause large changes (by several eV). Therefore, a systematic theoretical investigation is highly desirable to separate the migration energy barrier from the activation energy and provide valuable insights into the various atomistic migration processes.

The purpose of this work is to comprehensively investigate the diffusion of oxygen vacancies and interstitials in ZnO by first-principles calculation. A novel non-symmetric configuration of oxygen octahedral interstitials is found, presumably due to Jahn–Teller distortion. Oxygen octahedral interstitials are found to diffuse efficiently by the kick-out mechanism. Based on our calculation results, oxygen octahedral interstitials are fast diffusers, contributing to annealing processes, as well as being responsible for the self-diffusion of oxygen for n-type ZnO, and oxygen vacancies are responsible for the self-diffusion of oxygen for p-type ZnO.

2. Calculational method and models

The density functional calculations were carried out using the plane-wave based Vienna *ab initio* simulation package (VASP) [12, 13]. We perform our calculations within both the local density approximation (LDA) [14] and the generalized gradient approximation (GGA) [15, 16], since it is currently not understood which of these two flavors of density-functional theory give more accurate results. It is well known that LDA overbinds molecules and solids and underestimates bonds and

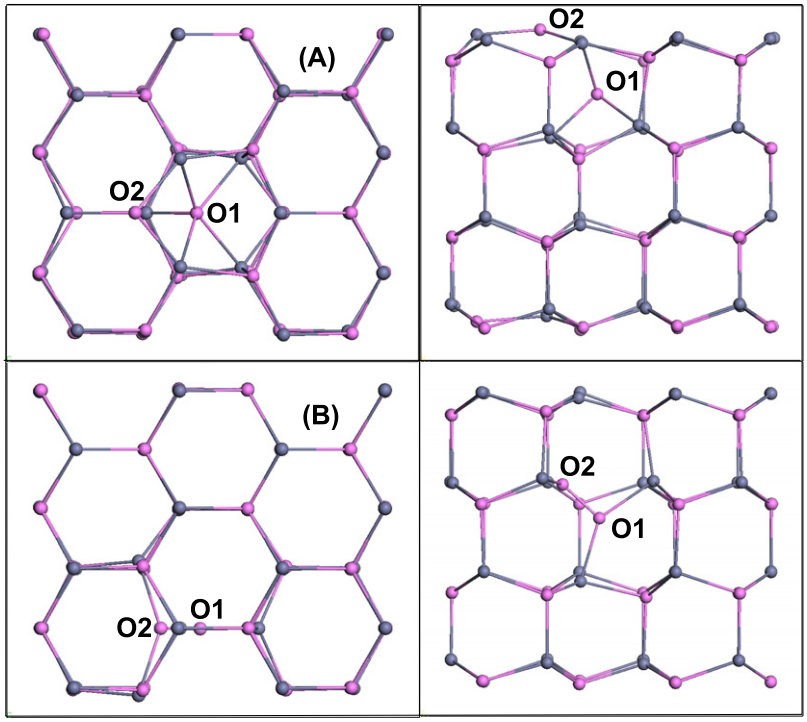

Figure 1. Atomic geometry of (A) non-symmetric octahedral interstitial (O_i^{2-}(oct)) and (B) split interstitial (O_i^0(split)). The left side is the top view along the *c* axis; the right side is the side view perpendicular to the *c* axis (GGA).

lattice distances, while GGA methods correct and sometimes overcorrect this. The difference between the results gives us an estimate of the error introduced by the exchange–correlation functional. The electron wavefunctions were described using the projector augmented wave (PAW) method of Blöchl [17] in the implementation of Kresse and Joubert [18]. Plane waves have been included up to a cutoff energy of 400 eV. Electronic states were occupied with a Gaussian smearing width of 0.05 eV. A real-space projection scheme was used for efficient computations. Orthogonal supercells containing 96 atoms were employed, with $a_1 = 11.07$ Å, $a_2 = 9.59$ Å, $a_3 = 10.32$ Å for LDA and with $a_1 = 11.38$ Å, $a_2 = 9.85$ Å, $a_3 = 10.59$ Å for GGA, which have lattice vectors $(0, 2\sqrt{3}a, 0)$, $(3a, 0, 0)$, $(0, 0, 2c)$. All calculations were carried out at the theoretical constant of bulk wurtzite ZnO. For integration within the Brillouin zone specific *k* points were selected using $2 \times 2 \times 2$ Monkhorst–Pack grids. The optimization procedure was truncated when the residual forces for the relaxed atoms were less than 0.01 eV Å^{-1}. The zinc 3d electrons were explicitly included in our calculations.

In order to obtain the energy barriers for the various diffusion paths we employed the climbing image nudged elastic band method [19, 20] as implemented in VASP by Henkelman, Jonsson, and others [21], which is expected to be more reliable than dragging an atom from minimum to minimum across the estimated or guessed saddle point, especially in multiatom migration events. The images of CI-NEBM were relaxed until the maximum residual force was less than 0.01 eV Å^{-1}. For the charged state, a neutralizing background charge was imposed automatically in VASP calculations. The dynamic charged effect and bandgap correction are excluded from our consideration.

3. Results

3.1. Atomic geometry

3.1.1. Oxygen vacancy. The stable charge state of an oxygen vacancy under n-type conditions and p-type conditions is 0 and +2 [10]. The +1 charge state is unstable. For the 0 charge state, the oxygen vacancy shows inward relaxation. The Zn–Zn bond lengths about the oxygen vacancy shorten on average by about 12% (LDA) or 9% (GGA). For the +2 charge state, the oxygen vacancy shows an outward relaxation. The Zn–Zn bond lengths about the oxygen vacancy extend on average by about 23% (LDA) or 23% (GGA).

3.1.2. Oxygen interstitial. The stable charge state of the oxygen interstitial under n-type conditions and p-type conditions is −2 and 0 [10]. The −1 charge state is only stable under semi-insulating conditions. It is excluded from our consideration.

For the −2 charge state, the most stable configuration is the oxygen octahedral interstitial (O_i^{2-}(oct)). A novel non-symmetric configuration is found, as shown in figure 1(A), with 0.08 eV (0.16 eV) lower energy compared with the symmetric configuration for LDA (GGA). We can see that oxygen atom O1 approaches O2, then O2 is noticeably pushed upwards. It seems necessary to explain why previous studies have not found this configuration. This non-symmetric configuration is found during investigation of the diffusion of O_i^{2-}(oct) perpendicular to the *c* axis. Previous studies [9, 10] have not calculated such a process.

For the 0 charge state, the most stable configuration is the split interstitial, O_i^0(split), called the dumbbell interstitial [9],

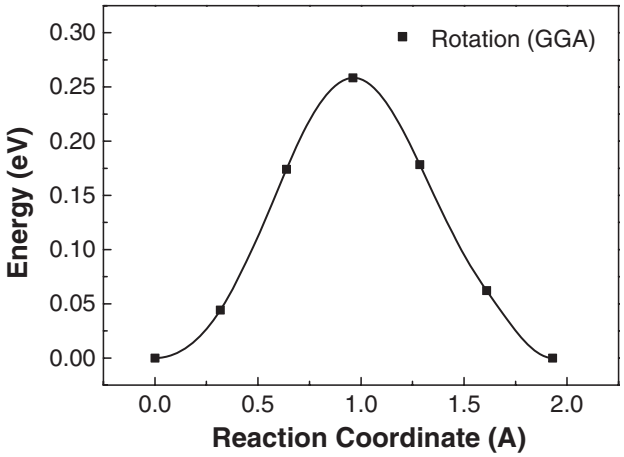

Figure 2. Calculated energy along the rotation process of the oxygen interstitial O_i^0(split) by 120° around the *c* axis.

as shown in figure 1(B), which possesses a threefold symmetry axis; i.e., rotations about the *c* axis by multiples of 120° generate equivalent configurations. We find that the metastable configuration, $O_i^0(\text{split})^*$, called the rotated dumbbell interstitial [9], reported in [9] and [10] is very unstable. This rotated dumbbell interstitial can be obtained by rotating the dumbbell interstitial by 60°, as pointed out by Erhart and Albe [9]. Erhart and Albe [9] found there is a smaller than 0.1 eV energy barrier of transformation from the rotated dumbbell interstitial to dumbbell interstitial. Here, we investigated the rotation process from one dumbbell interstitial to another dumbbell interstitial by 120° (GGA) to reveal these issues. We can see that there is no obvious metastable state during the process, as shown in figure 2. Using the configuration of the saddle point as the initial configuration, the rotated dumbbell interstitial can be obtained. This so-called rotated dumbbell interstitial has 0.26 eV higher energy than the dumbbell interstitial (GGA), consistent with the results of Janotti and Walle [10], which is 0.2 eV (LDA). Therefore, the rotated dumbbell interstitial is excluded from our consideration.

3.2. Diffusion of oxygen vacancy

For vacancy mechanisms, a nearest neighbor oxygen atom in the oxygen lattice jumps into the adjacent vacant site, leaving a vacancy behind. There are two migration pathways, parallel and perpendicular to the *c* axis, corresponding to out-of-plane and in-plane diffusion [9]. Calculated energies along the migration paths are shown in figure 3. We can see that the charge state has a large effect on the diffusion of oxygen vacancy. The energy barrier of in-plane diffusion of V_O^0 is 2.44 (LDA) or 2.06 eV (GGA) and the energy barrier of out-of-plane diffusion of V_O^0 is 2.77 (LDA) or 2.34 eV (GGA). There are about 0.3 eV energy difference between in-plane and out-of-plane diffusion for both LDA and GGA. The energy barrier of in-plane diffusion of V_O^{2+} is 1.21 (LDA) or 1.44 eV (GGA), and the energy barrier of out-of-plane diffusion of V_O^{2+} is 1.56 (LDA) or 1.46 eV (GGA). There is about 0.3 eV energy difference between in-plane and out-of-plane diffusion for LDA, whereas there is almost no energy difference for GGA.

3.3. Diffusion of oxygen interstitial under n-type conditions

Under n-type conditions, the stable charge state of the oxygen interstitial is −2, and the most stable configuration is the oxygen octahedral interstitial. There are two types of diffusion mechanisms for the interstitial type defect, including interstitial mechanisms and kick-out mechanisms.

For interstitial mechanisms, the oxygen interstitial migrates directly from one lattice interstice to another adjacent lattice interstice. We have considered two migration paths for O_i^{2-}(oct), parallel and perpendicular to the *c* axis, respectively, as shown in figure 4((a) and (b)). For diffusion perpendicular to the *c* axis, the oxygen interstitial diffuses directly from the most stable non-symmetric configuration to the adjacent non-symmetric oxygen interstitial, with energy barrier of 0.81 (LDA) or 0.89 eV (GGA), as shown in figure 5. For diffusion parallel to the *c* axis, the oxygen interstitial first transforms to the symmetric configuration, then diffuses along the hexagonal channel to another symmetric oxygen interstitial, and then relaxes to the most stable non-symmetric configuration. Surprisingly, we have found two different

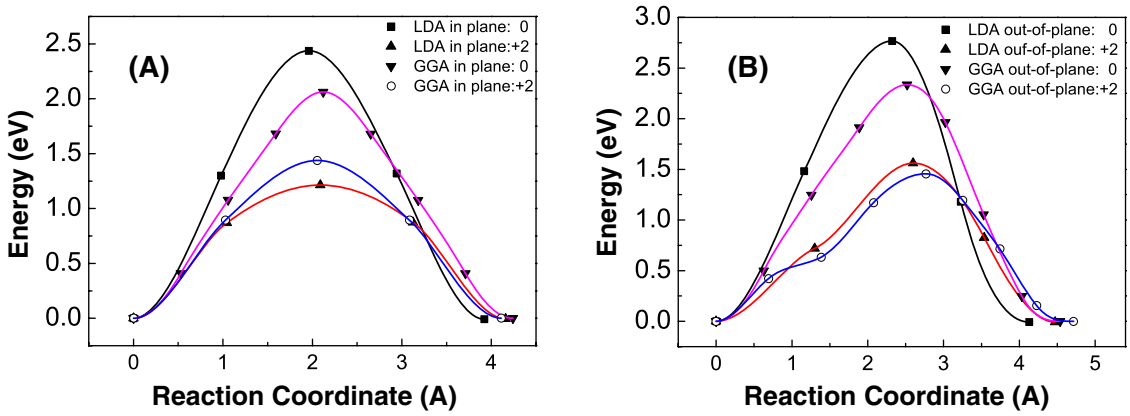

Figure 3. Calculated energy of oxygen vacancy migration: (A) perpendicular to the *c* axis (in plane) and (B) parallel to the *c* axis (out of plane).

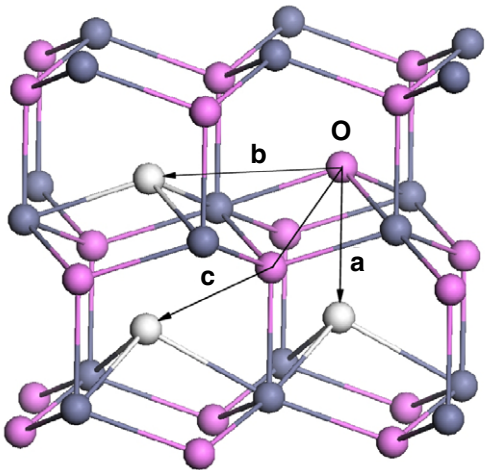

Figure 4. Schematic illustration of diffusion paths for oxygen interstitial O_i^{2-}(oct). (a) Diffusion parallel to the *c* axis. (b) Diffusion perpendicular to the *c* axis. (c) Kick-out process.

pathways for this process. One has similar energy barrier, 0.89 (GGA), to the perpendicular diffusion, whereas the other has much smaller energy barrier, 0.60 (LDA) or 0.52 eV (GGA), as shown in figure 5(A). We do not consider the former pathway further. The overall energy barrier of the latter pathway is 0.68 eV both for LDA and GGA.

For kick-out mechanisms, the oxygen octahedral interstitial moves towards a substitutional O, replaces it and kicks it into an adjacent octahedral interstitial, as shown in figure 4(c). It is found that the oxygen interstitial first transforms to the symmetric configuration, and then goes downwards to a substitutional O, replaces and pushes it to the most stable non-symmetric configuration. The calculated energy along the migration path is shown in figure 5(B). To understand this process, let us consider the reverse process, as shown in figure 1(A): it is obvious that it is easy for O1 to kick O2 out to the interstitial site, since O2 has been noticeably pushed upwards. The overall migration barrier is 0.48 (LDA) or 0.49 eV (GGA). In addition, the split interstitial has about 1.54 eV (LDA) or 1.25 eV (GGA) higher energy than the most stable non-symmetric configuration, so it is excluded as intermediate state from our consideration.

3.4. Diffusion of oxygen interstitial under p-type conditions

Under p-type conditions, the stable charge state of the oxygen interstitial is 0, and the most stable configuration is the split interstitial, O_i^0(split), as shown in figure 1(B). We have considered two migration paths for O_i^0(split), parallel and perpendicular to the *c* axis. As seen in figure 1(B), O1 can diffuse parallel and perpendicular to the *c* axis to join an adjacent O sublattice site and forms a new split interstitial. For diffusion perpendicular to the *c* axis, there are several possible pathways, corresponding to O1 and O2 diffusion away from the split interstitial. However, we found that they have almost the same energy barriers, as shown in figure 6(B), 'GGA per down'(O1) and 'GGA per up'(O2). The energy barrier of diffusion parallel and perpendicular to the *c* axis is 1.09 eV (LDA) or 1.02 eV (GGA), 1.16 eV (LDA) or 1.08 eV (GGA), respectively. The diffusion is almost isotropic. The energy barrier of on-site rotation of the split interstitial is 0.26 eV (GGA). In addition, the energy of the O_i^0(oct) is about 1.37 eV (LDA) or 1.54 eV (GGA) higher than the O_i^0(split), so it is excluded as intermediate state from our consideration.

3.5. Influence of GGA + U on the diffusion barrier

In this part, we try to illustrate the influence of GGA + *U* on the diffusion barrier. Erhart and Albe [9] used GGA + *U* to calculate the diffusion barrier, and found that the migration energy for the lowest energy paths obtained with GGA and GGA + *U* differ by at most 0.3 eV. On the other hand, Janotti and Walle [10] found that the values calculated with LDA and LDA + *U* differed by less than 0.1 eV, and their results are all obtained within the LDA. In order to reveal the influence of GGA + *U* on the diffusion barrier, we only investigated the novel kick-out process of O_i^{2-}(oct). The calculation was carried out at the theoretical constant of bulk wurtzite ZnO with effective *U* parameter $U_{\text{eff}} = 7.5$ eV. The calculated energy along the process is shown in figure 7. The overall kick-out energy barrier is 0.54 eV (GGA + *U*), differing by less than 0.1 eV from GGA results (0.49 eV). The influence of GGA+*U* on the diffusion barrier can be ignored.

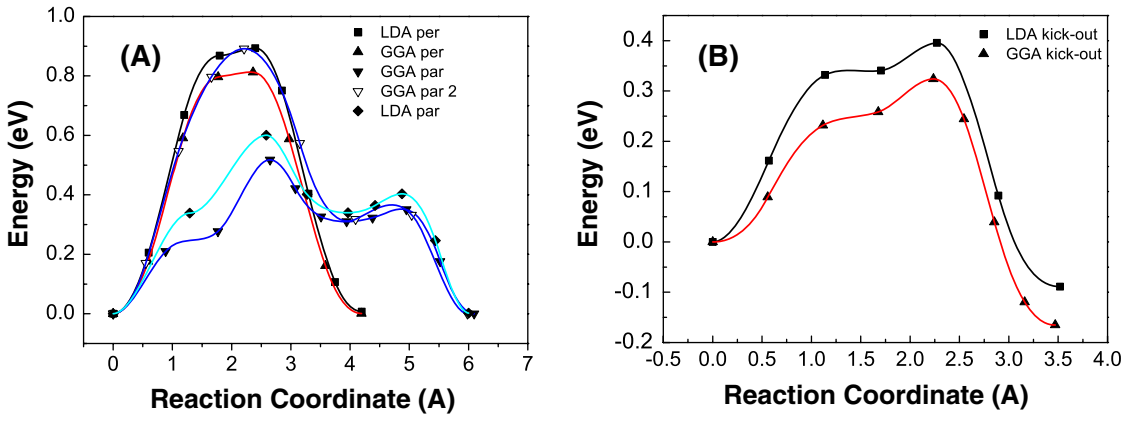

Figure 5. Calculated energy of oxygen octahedral interstitial O_i^{2-}(oct) migration: (A) interstitial mechanisms and (B) kick-out mechanisms.

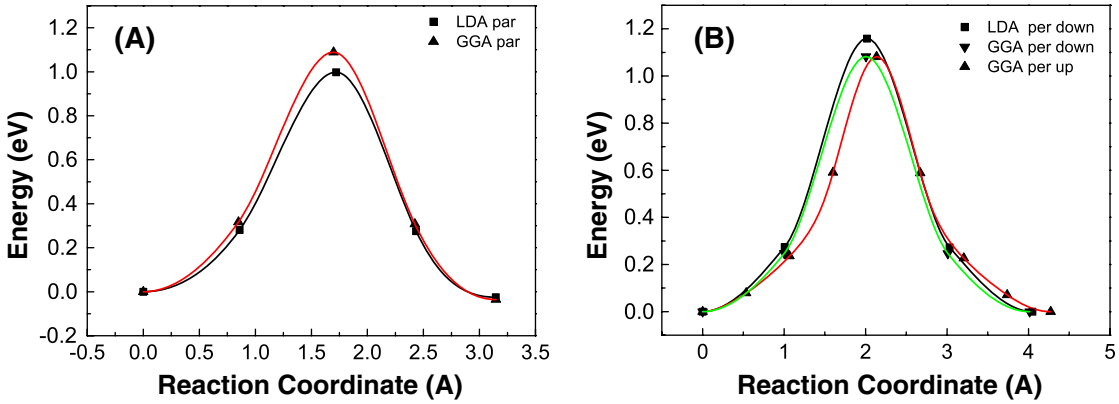

Figure 6. Calculated energy of oxygen interstitial O_i^0(split) migration: (A) parallel to c axis and (B) perpendicular to c axis.

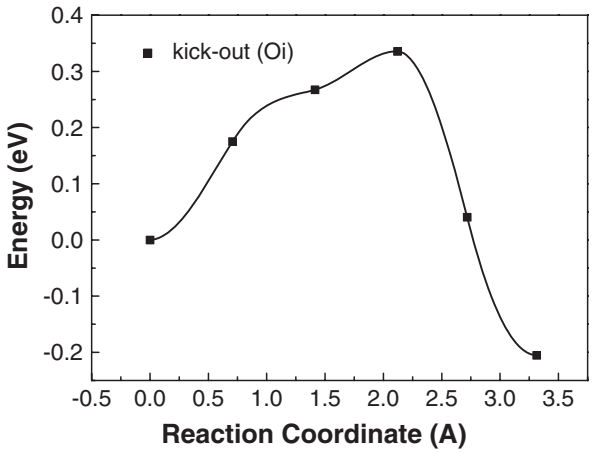

Figure 7. Calculated energy along the kick-out process of the oxygen interstitial O_i^{2-}(oct) for GGA + U ($U_{\text{eff}} = 7.5$ eV).

Table 1. Calculated and reported migration energy barriers E_b.

Migration path		E_b (eV)			
		LDA	GGA	LDA [10]	GGA + U [9]
In plane	V_O^0	2.44	2.06	2.4	1.87
Out of plane	V_O^0	2.77	2.34	2.4	2.55
In plane	V_O^{2+}	1.21	1.44	1.7	1.49
Out of plane	V_O^{2+}	1.56	1.46	1.7	1.09
$\perp$ c axis (per)	O_i^{2-}(oct)	0.81	0.89		
$\parallel$ c axis (par)	O_i^{2-}(oct)	0.68	0.68	1.1	
Kick-out	O_i^{2-}(oct)	0.48	0.49		
$\perp$ c axis (per)	O_i^0(split)	1.16	1.08	0.9	0.95
$\parallel$ c axis (par)	O_i^0(split)	1.09	1.02	0.9	0.81

4. Discussion

All of the related energy barriers are summarized in table 1. We can see that charge state has large effects on the diffusion of the oxygen vacancy. The LDA and GGA results generally differ by about 0.1–0.3 eV. For V_O^0, there is about 0.3 eV energy difference between in-plane and out-of-plane diffusion both for LDA and GGA. This indicates that some anisotropic behaviors would be present. However, for V_O^{2+}, the LDA and GGA results differ from each other. For LDA, there is about 0.3 eV energy difference between in-plane and out-of-plane diffusion. For GGA, there is almost no anisotropy between them. Janotti and Walle [10] have also investigated the diffusion of the oxygen vacancy, and found no anisotropy, whereas Erhart and Albe [9] found large anisotropy. Based on our results, the diffusion of V_O^0 is more or less anisotropic, but it is not very clear whether V_O^{2+} is anisotropic or not. For diffusion of O_i^{2-}(oct), we found that it tends to occur via the kick-out mechanism, with 0.48 (LDA) or 0.49 eV (GGA) energy barrier. This conclusion is noticeably different from previous calculations [9, 10]. It seems necessary to explain the origin of these differences. Erhart and Albe have not investigated the diffusion of O_i^{2-}(oct) [9]. Janotti and Walle have considered this process, but have not actually calculated the kick-out process (see page 16 of [10]). (They counted on intuition for this process.) That is to say, we find a novel small energy barrier migration path, which is not contrary to previous studies [9, 10]. For diffusion of O_i^0(split), the energy barrier is about 1.0–1.2 eV, fairly close to previous calculations [9, 10].

The activation energy for self-diffusion is the sum of the formation energy of the defect that mediates the self-diffusion and its migration energy barrier [11]. The Fermi level does not affect the diffusion barriers directly, but determines the thermal stable charge state and affects the formation energy. Most experiments are performed in Zn-rich conditions [10]. Under extremely n-type conditions, the formation energy of V_O^0, V_O^{2+}, O_i^{2-}(oct) and O_i^0(split) is about 3.72, 6, 4 and 5.24 eV [10], and the corresponding activation energy is roughly 6, 7, 4.5 and 6 eV. (V_O^{2+} is not stable at n-type conditions, but it just indicates that it has larger formation energy. So it is also included in the n-type condition.) In contrast to the results of Janotti and Van de Walle, O_i^{2-}(oct) is expected to be responsible for the self-diffusion of oxygen in ZnO under n-type conditions. Under p-type conditions, the formation energy of V_O^{2+}, O_i^{2-}(oct) and O_i^0(split) is about 0, 10.86 and 5.24 eV [10], and the corresponding activation energy is roughly 1.3, 11 and 6 eV. Thus, under p-type conditions, oxygen self-diffusion will be mediated by V_O^{2+}.

The migration energy barrier of O_i^{2-}(oct) is rather small, about 0.5 eV. It is expected to contribute to the defect annealing at low temperature and remarkable radiation hardness of zinc oxide.

5. Conclusion

We have performed a detailed first-principles study of the diffusion mechanism of the oxygen vacancy and interstitial. The migration barrier of the oxygen octahedral interstitial O_i^{2-}(oct) is very small, about 0.5 eV, which implies that it should be mobile down to very low temperature. Based on our calculation results, the oxygen octahedral interstitial can diffuse efficiently by the kick-out mechanism, and is responsible for the self-diffusion of oxygen for n-type ZnO, which is a novel finding. On the other hand, oxygen vacancies are responsible for the self-diffusion of oxygen for p-type ZnO.

Acknowledgment

The work is supported by the 973 Project (Ministry of Science and Technology of China, grant No 2006CB605102).

References

[1] Ozgur U, Alivov Y I, Liu C, Teke A, Reshchikov M A, Dogan S, Avrutin V, Cho S J and Morkoc H 2005 *J. Appl. Phys.* **98** 041301
[2] Bozdog C, Przybylinska H, watkins G D, Harle V, Scholz F, Mayer M, Kamp M, Molnar R J, Wickenden A E, Koleske D D and Henry R L 1999 *Phys. Rev.* B **59** 12479
[3] Moore W J and Williams E L 1959 *Discuss. Faraday Soc.* **28** 86
[4] Hoffman J W and Lauder I 1970 *Trans. Faraday Soc.* **66** 2346
[5] Robin R, Cooper A R and Heuer A H 1973 *J. Appl. Phys.* **44** 3770
[6] Tomlins G W, Routbort J L and Mason T O 1998 *J. Am. Ceram. Soc.* **81** 869
[7] Haneda H, Sakaguchi I, Watanabe A, Ishigaki T and Tanaka J 1999 *J. Electroceram.* **4** 41
[8] Sabioni A C S, Ramos M J F and Ferraz W B 2003 *Mater. Res.* **6** 173
[9] Erhart P and Albe K 2006 *Phys. Rev.* B **73** 115207
[10] Janotti A and Van de Walle C G 2007 *Phys. Rev.* B **76** 165202
[11] Glicksman M E 2000 *Diffusion in Solids: Field Theory, Solid-State Principles and Applications* (New York: Wiley)
[12] Kresse G and Hafner J 1993 *Phys. Rev.* B **47** 558
[13] Kresse G and Furthmuller J 1996 *Phys. Rev.* B **54** 11169
[14] Perdew J P and Zunger A 1981 *Phys. Rev.* B **23** 5048
[15] Perdew J P, Chevary J A, Vosko S H, Jackson K A, Pederson M R, Singh D J and Fiolhais C 1992 *Phys. Rev.* B **46** 6671
[16] Perdew J P, Chevary J A, Vosko S H, Jackson K A, Pederson M R, Singh D J and Fiolhais C 1993 *Phys. Rev.* B **48** 4978
[17] Blöchl P E 1994 *Phys. Rev.* B **50** 17953
[18] Kresse G and Joubert D 1999 *Phys. Rev.* B **59** 1758
[19] Henkelman G, Jhannesson G and Jonsson H *Progress on Theoretical Chemistry and Physics* 2000 (Dordrecht: Kluwer Academic) p 269
[20] Henkelman G, Uberuaga B P and Jonsson H 2000 *J. Chem. Phys.* **113** 9901
[21] The implementations of the climbing image nudged elastic band and the dimer method for VASP were obtained from http://theory.cm.utexas.edu/henkelman